RSC Advances

ROYAL SOCIETY OF CHEMISTRY

www.rsc.org/advances

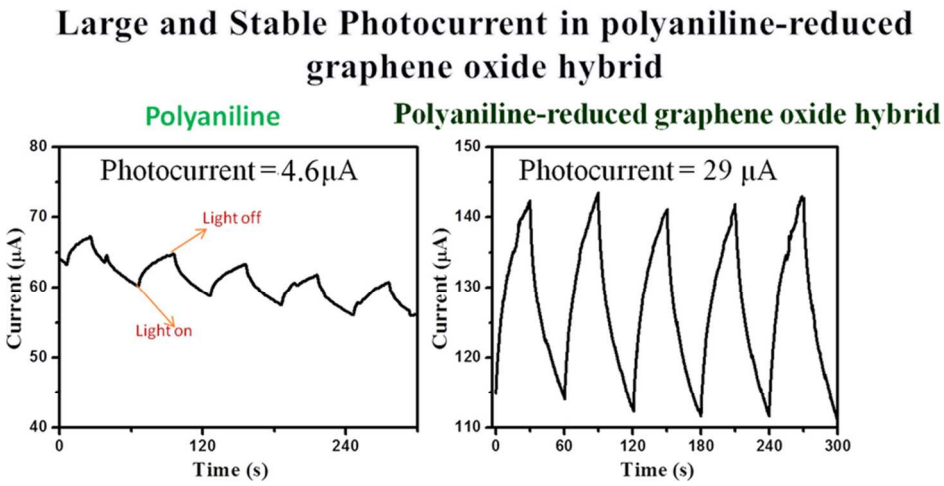

40x20mm (600 x 600 DPI)

RSC Advances

Dynamic Article Links ►

Cite this: DOI: 10.1039/c0xx00000x

www.rsc.org/xxxxxx

ARTICLE TYPE

Phenylenediamine functionalized reduced graphene oxide/polyaniline hybrid: Synthesis, characterization, improved conductivity and photocurrent generation

Remyamol T,[a] Pramod Gopinath[b] and Honey John*[a]

Received (in XXX, XXX) Xth XXXXXXXXX 20XX, Accepted Xth XXXXXXXXX 20XX
DOI: 10.1039/b000000x

Phenylenediamine functionalized reduced graphene oxide (GONH2) is designed and synthesized for the preparation of polyaniline/reduced graphene oxide hybrid having better interactions than that of unfunctionalized graphite oxide/polyaniline hybrid. Hybrids are synthesized by the *in situ* polymerization of aniline in the presence of GONH2. Defects generated in GONH2 during functionalization are repaired during hybrid formation. Due to the presence of free amino groups in GONH2, it will participate in the polymerization of aniline and covalent bonds will be formed between polyanline and GONH2, resulting in the increased room temperature conductivity and photocurrent generation compared to pure polyaniline and polyaniline/graphite oxide hybrid synthesized in the same experimental conditions. Significant reduction and exfoliation of graphite oxide after functionalization with phenylenediamine, formation of direct conducting pathways by covalent connections and the photoinduced electron transfer between polyaniline and GONH2 plays a major role for the improved electrical conductivity and photocurrent generation.

Cite this: DOI: 10.1039/c0xx00000x

www.rsc.org/xxxxxx

ARTICLE TYPE

1. Introduction

Graphene, the single layered graphite with conjugated hexagonal lattice, is the nearly ideal 2D material[1, 2]. The optoelectronic and light harvesting applications of graphene are of particular interest for academic, technological and industrial sectors. A major challenge in developing light harvesting devices is the effective separation of photogenerated electron-hole pairs and the transfer of electron to the electrode. Graphene is a promising electron acceptor material[3] for the photocurrent generating devices due to its high specific surface area, tunable bandgap and the higher linear in-plane dimensions (approximately 5 µm) compared to the thickness (0.34 nm)[4-6]. The photoinduced electron transfer from various semiconducting materials to carbon materials like carbon nanoparticles[7], carbon quantum dots[8], graphene[9], etc. have been recently demonstrated for photovoltaic and photocatalytic applications. To date various synthetic methods, like mechanical exfoliation, epitaxial growth, chemical and electrochemical reduction of graphite oxide (GO), etc. have been developed for producing high quality graphene[3,10-14]. Among them the chemical reduction of GO is proven to be the effective method because of the low cost and possibility of mass production. Heavy oxygenation of graphite during GO synthesis[15] results in different functional groups (hydroxyl, carboxy, epoxy and alkoxy groups) on the basal planes and the edge sites and makes GO sheets strongly hydrophilic and easily dispersible[16-18], hence opens up a way to introduce various functional materials. Recently graphene based composite materials of metal and metal oxide nanoparticles[19-22], nanoparticles of semiconducting oxides[23,24], quantum dots[25], conducting polymers[26-28], etc. are gaining more attraction due to the synergetic combination of properties of different components. The challenge in designing composite systems is the requirement to obtain defect free individual graphene oxide or graphene sheets in the reduced form. Conducting polymer/graphene hybrids are a major class of composite materials for the fabrication of donor/acceptor based electronic devices[29-32]. Among conducting polymers, polyaniline being an excellent organic conductor with good environmental stability and low cost, has often been used to make composite with carbonaceous materials, especially with graphene. Mainly polyaniline/graphene hybrids are synthesized by noncovalent mixing or covalent grafting. Both methods have its own advantages and disadvantages.

The covalently connected graphene-porphyrin hybrids have been recently studied for photocurrent generation applications. Karousis et al.[33] electrophoretically deposited graphene oxide with covalently linked porphyrin antennae on tin oxide and the electrode exhibits an incident photon-to-photocurrent-efficiency of 1.3% in a standard photoelectrochemical cell. Tang et al.[34] very recently synthesized porphyrin hybrid covalently functionalized with graphene and studied the improved photocurrent generation compared to free porphyrin. Eventhough covalently grafted hybrids of graphene are known in the literature for photocurrent generation applications, the advantages of covalently connected polyaniline–graphene hybrids are not highly explored. Few papers are published specially aiming supercapacitor applications[35-39], memory effect[40] and optical limiting[41] of polyaniline-graphene hybrids with covalent interactions.

Herein we report the phenylenediamine functionalization of GO (synthesis of GONH2) followed by the hybridization with polyaniline. Phenylenediamine functionalization is designed to achieve covalent linkage between polyaniline and reduced graphene oxide in the simple one step polymerization reaction. Considerable reduction and exfoliation of GO is achieved after functionalization and Raman spectrum suggests the repairing of defects after hybridization with polyaniline. Significant electron transfer between polyaniline and GONH2 is evidenced by the photoluminescence quenching of polyaniline after hybrid formation. The hybrid shows considerable improvement in dc-conductivity and photocurrent compared to pure polyaniline.

2. Experimental

2.1. Materials

Graphite powder with particle size less than 20 µm was purchased from Sigma Aldrich and used as such for the synthesis of GO. All the other chemicals used were purchased from Merck India. Aniline, thionyl chloride and dimethyl formamide were distilled prior to use and other chemicals were used as such.

2.2. Characterization

Fourier Transform Infra-red (FTIR) spectra were recorded using Perkin Elmer 100 FTIR spectrometer. X-ray diffraction (XRD) studies and X-ray photoelectron spectroscopy (XPS) were performed using Bruker AXS D8 advance X-ray diffractometer using Cu Kα (λ = 1.54 Å) radiation and Kratos Axis ultra photoelectron spectrometer with a monochromatic Al Kα X-ray source respectively. The Raman spectrum of the samples were recorded in WiTech alpha 300 Raman spectrometer excited with 488 nm. Thermal studies were done using thermogravimetric analysis (TGA Q50, TA instruments) at a heating rate of 10 ^{o}C under nitrogen atmosphere. Morphology of the samples were studied using FEI Quanta FEG 200 high resolution scanning electron microscope (HRSEM) and FEI Quanta high resolution transmission electron microscope (HRTEM). UV-visible spectra were recorded using Carey100 Bio UV–Visible spectrophotometer. Cyclic Voltametry was performed on an Autolab electrochemical workstation with a three electrode cell in a solution of NaCl (0.1 M) at a scan rate of 100 mV/ s. The m-cresol solution of the sample was drop cast onto the glassy carbon electrode and then dried at 100 ^{o}C to form a thin film. A Pt wire was used as the counter electrode, and a $Ag/AgNO_3$ electrode was used as the reference electrode.

2.3. Electrical conductivity measurements

The dc-conductivity of the samples, in the form of circular pellets, were measured at room temperature using four-probe method. The current from a dc-source meter (Keithley, 2182A) was allowed to pass through the outer probes of the four-probe and voltage across the two inner probes was measured using Keithley nanovoltmeter (6221). The dc-conductivity is calculated using the standard van der Pauw relation

$$\rho = (\ln 2/\pi t)(I/V)$$

where t is the thickness of the sample and is taken as the average of three different measurements using a screw gauge. The equation can be applied only if the sample size is large compared to the probe spacing (d/s>40), hence in order to get accurate measurements correction for the edge effects is required. For our studies, we used circular pellets of the samples with a diameter of 13 mm and thickness less than 0.5 mm. The probe spacing used was 2 mm. So edge correction of 0.82 was applied to the above equation. The pellets of the samples were prepared by applying a pressure of 4 tons using a hydraulic press (PCI Analytics Pvt. Ltd, Mumbai). The correction factor is obtained from the National Bureau of Standards Technical Note 199 – "Correction Factor Tables for Four-Point Probe Resistivity Measurements on Thin, Circular Semiconductor Samples".

2.4. Photocurrent measurements

Thin films of the samples were fabricated on clean FTO glasses. The FTO glasses were cleaned by ultrasonication in acetone, methanol and distilled water. The samples in a cresol/nafion mixture were spin coated on FTO at 1500 rpm for 1 min. After spin coating, the films were baked at 100 ^{o}C for 30 min.

Photocurrent experiments were conducted with Autolab electrochemical work station in a conventional three electrode electrochemical cell comprising of the thin film sample as the working electrode, platinum wire as counter electrode and Ag/AgCl as a reference electrode. 0.2 M Na_2SO_4 taken in a quartz beaker was used as the electrolyte solution. The electrolyte was bubbled with nitrogen before and during the measurement. The active area of the working electrode was 0.25 cm^2. The potential of the working electrode was set at 3 V. An incandescent lamp operating at 300 W was used as the illumination source and the photointensity was measured using digital solar meter (Daystar meter, USA) which uses polycrystalline silicon photovoltaic cell as the sensor. The light intensity chosen for the measurement was 100 mW/cm^2.

2.5. Synthesis and phenylenediamine functionalization of GO and the hybrid formation with polyaniline

GO was synthesized by the oxidation of graphite by low temperature modified Hummers method[15] and it is functionalized with phenylenediamine by the formation of amide linkages. The hybrids were synthesized by the *in situ* polymerization of aniline in the presence of GONH2. The aniline:GONH2 ratio was chosen as 1:2 and the hybrid was named as P1NH2G2. Because of the presence of phenylenediamine groups, the GONH2 can participate in the polymerization of aniline. The chains initiated by the phenylene diamine radical cation will get covalently grafted into the reduced graphene oxide layers, while the chains initiated by the aniline radical cations will get physically trapped in reduced graphene oxide layers. The detailed synthesis procedure is reported earlier[41].

2.6. Synthesis of polyaniline/GO hybrid

In order to study the improved properties of the hybrid by the formation of covalent bonds between polyaniline and GONH2, polyaniline/GO hybid was synthesized as a control sample using GO, instead of GONH2, keeping other conditions the same. The hybrid is named as P1G2.

3. Results and Discussion

3.1. Characterization of GO and GONH2

The presence of oxygen functionalites in GO is characterized using FTIR spectrum. Figure 1 (a) shows the FTIR spectrum of graphite, GO and GONH2.

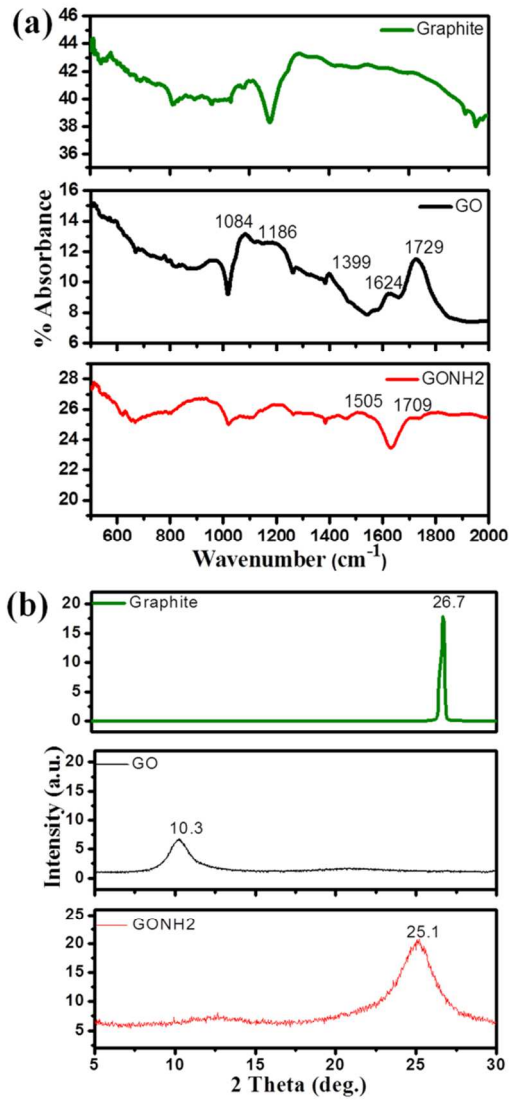

Fig. 1 (a) FTIR spectrum and (b) XRD spectrum of graphite, GO and GONH2

In GO, the peak observed at 1729 cm^{-1} is due to the carbonyl stretching vibration of carboxylic acid groups. The peaks at 1399, 1186 and 1084 cm^{-1} are due to the C-O stretching vibration of carboxy, epoxy and alkoxy groups, respectively[38]. The peak at 1624 cm^{-1} is ascribed to skeletal vibrations of unoxidized graphitic domain[42]. After functionalization with phenylenediamine, the peak corresponding to carbonyl stretching is shifted to 1709 cm^{-1} due to the formation of amide bonds. The characteristic N-H bending vibration at 1505 cm^{-1} is also recorded. XRD spectrum of samples are shown in figure 1 (b). Graphite shows characteristic peak at $2\theta=26.7^{o}$. After the introduction of oxygen functionalities, the graphitic peak shifts to 10.3^{o} with an increase of d-spacing to 0.86 nm. The increase in d-spacing is due the weakening of van der waals interaction between the layers because of the intercalation of oxygen functionalities. The disappearance of 0.34 nm inter-graphene spacing indicates the complete oxidation of graphite into GO.When phenylenediamine is grafted, the peaks at $2\theta=10.3^{o}$ disappears and a new broad peak appears at $2\theta=25.1^{o}$ due to the decrease of interlayer spacing by the removal of intercalated oxygen functional groups, hence indicating the reduction of GO after phenylenediamine functionalization. The broadening of the peak compared to the graphitic peak is due to the poor ordering in the stacking direction and hence suggests destacking of GO during grafting of phenylenediamine.

The decomposition pattern of the samples is studied by TGA analysis and shown in figure 2 (a). Graphite is stable in the temperature range up to 800 ^{o}C, where as GO shows a major weight loss from 150-200 ^{o}C due to the loss of labile oxygen functional groups[43]. The increased inter layer spacing also promotes the easy removal of oxygen functionalities. Weight loss after 680 ^{o}C is due to the degradation of sp^3 carbon atom. The 8% weight loss up to 150 ^{o}C is due to the loss of adsorbed water molecules. From the TGA analysis, oxygen percentage is calculated as 47% (weight loss in the temperature range 150-680 ^{o}C). The weight loss in this temperature range is significantly reduced after the phenylenediamine grafting due to the removal of oxygen groups. XPS and Raman spectrum of the samples are given in figure 2 (b) and (c) respectively. XPS spectrum of GO shows 47% oxygen content and after functionalization, oxygen percentage is drastically reduced (8%) and carbon percentage is increased (86%) compared to GO. The peak corresponding to nitrogen also appears at 400 eV. Raman spectrum of graphite shows an intense G band at 1574 cm^{-1} and a very small D band at 1357 cm^{-1}. The G band is associated with the doubly degenerate phonon mode (E_{2g} symmetry) at the Brillouin zone center and D band is the disorder induced band[44]. After oxidation, the intensity of D band increases due to the introduction of defects. The I_G/I_D ratio of GO is 0.91, which is a measure of disorder. After phenylenediamine grafting, the intensity of D band again increases and I_G/I_D ratio is decreased to 0.81 because of more defects.

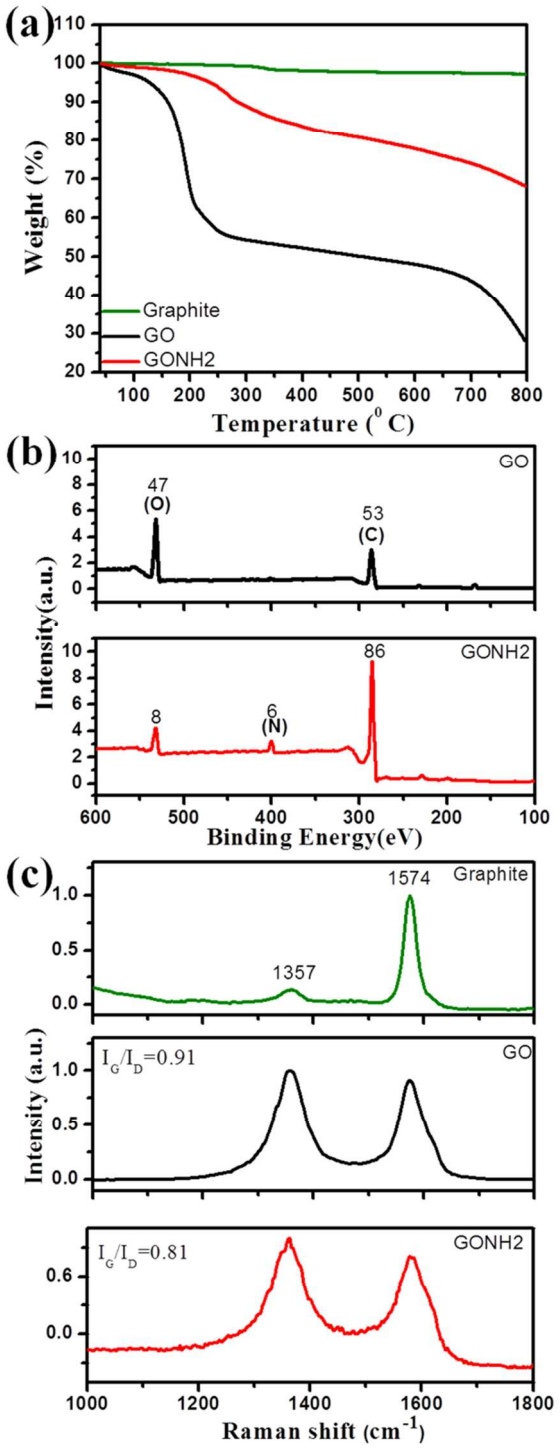

Fig. 2 (a) TGA pattern (b) XPS spectra and (c) Raman spectra of the samples.

SEM and TEM image of GO shown in figure 3 clearly depicts the layered and aggregated morphology of GO. The bumpy texture of the flat regions in SEM images can be related to the presence of isolated epoxy and hydroxyl reaction sites[45]. After the introduction of phenylenediamine, the surface become very rough and GONH2 shows wrinkled morphology. TEM image of

GONH2 clearly shows the considerable exfoliation of GO after phenylenediamine functionalization.

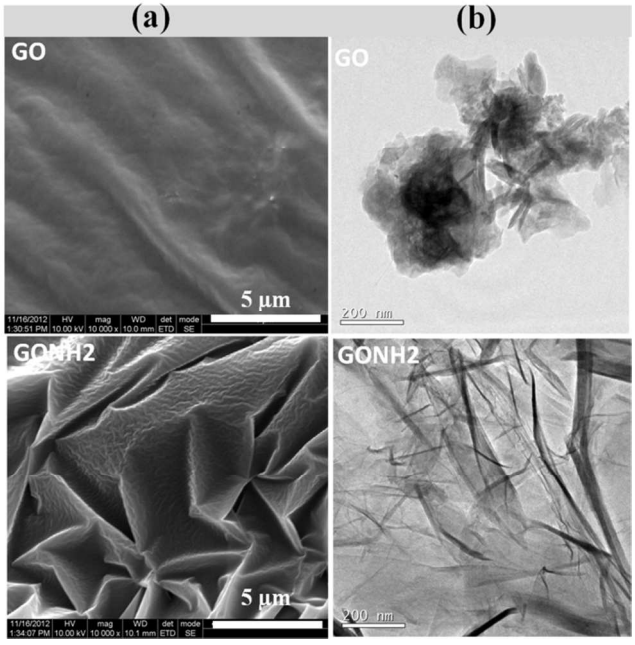

Fig. 3 (a) SEM images and (b) TEM images of GO and GONH2

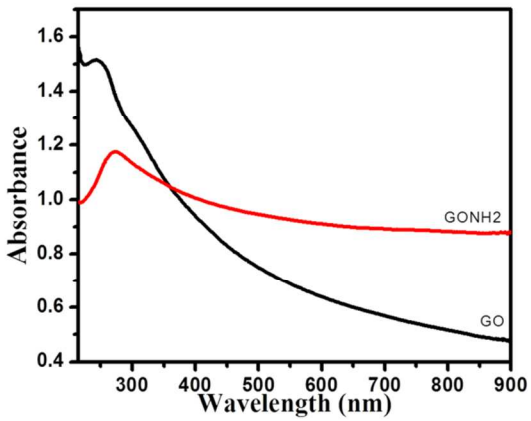

Fig. 4 UV-visible spectra of GO and GONH2

Figure 4 shows the UV-visible spectra of GO and GONH2 in 2-propanol. The spectrum of GO shows a peak at 244 nm corresponding to π-π* transition of C=C bond and a shoulder around 290-300 nm due to the n-π* transition of C=O bond.The absorption of GO at 244 nm is red shifted to 274 nm after diamine functionalization, indicating that the electronic conjugation is revived after phenylenediamine functionalization due to the reduction of GO[11]. All the above characterization techniques reveal the significant reduction and exfoliation of GO after phenylenediamine grafting, hence it is named as phenylenediamine functionalized reduced graphene oxide.

3.2. Characterization of polyaniline-GONH2 hybrid

Polymerization of aniline is carried out in the presence of GONH2 for the formation of hybrid. The structure of the hybrid is characterized by FTIR, XRD, TGA, and XPS analysis and is shown in figure 5 (a-d).

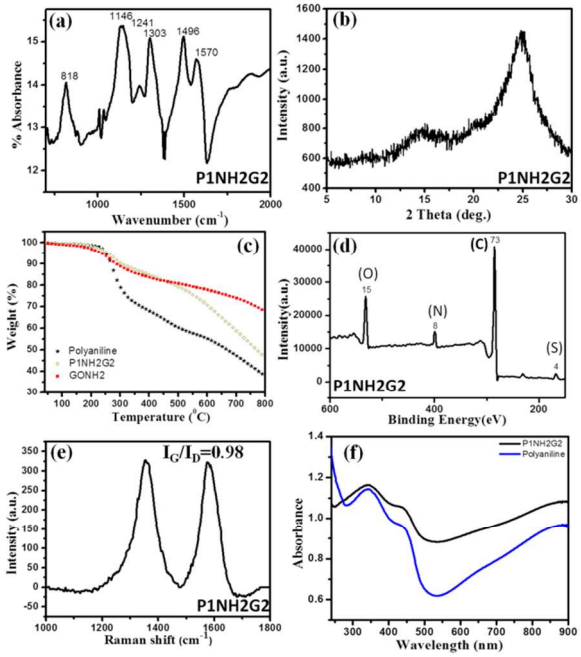

Fig. 5 (a) FTIR spectrum (b) XRD spectrum (c) TGA analysis (d) XPS spectrum (e) Raman spectrum and (f) UV-visible spectrum of the samples

The FTIR spectrum of the hybrid shows all the characteristic peaks of polyaniline, but is shifted to higher wavenumber side because of the π-π interaction of polyaniline with aromatic region of GONH2. The FTIR spectrum of polyaniline is shown in figure S1 (Supplementary Information) for a comparison. In figure 5 (a), the peak at 1570 and 1496 cm^{-1} are due to the C=C stretching vibration of the quinonoid and benzenoid rings of polyaniline. C-H in-plane and out-of-plane bending vibration are seen at 1146 and 818 cm^{-1}, respectively. C-N stretching vibrations of polaronic and nonpolaronic structures are found at 1241 and 1303 cm^{-1} respectively. The XRD spectrum of the hybrid (figure 5 (b)) shows the characteristic peaks of polyaniline at 15° and 25° corresponding to (011) and (200) plane respectively. The intensity of the characteristic peak of polyaniline at 2θ=20° (figure S2) corresponding to the periodicity parallel to the polymer chain is reduced in the hybrid spectrum because of the better π-π stacking in the hybrid. The peak corresponding to GO at 10.3° completely disappears in the spectrum of polyaniline-GONH2 hybrid. This clearly indicates the successful reduction of GO in the hybrids synthesized by this novel methodology. The decomposition pattern of the hybrid plotted along with that of polyaniline, hybrid and GONH2 are shown in figure 5 (c). Compared to pure polyaniline (38%), the hybrids show more residue (47%) because of the presence of stable GONH2. The XPS spectrum of the hybrid shown in figure 5 (d) reveals all the elements present in the hybrid (O, C, N and S). Raman spectrum of the hybrid shows increased I_G/I_D ratio (0.98), hence reduced disorder. This suggests defect repairing of GONH2 after hybrid formation with polyaniline resulting in larger sp^2 domain and extended π-conjugation. Figure 5 (f) shows the UV-Visible

spectra of polyaniline and the hybrid P1NH2G2 recorded in 2-propanol. The hybrid spectrum shows all the three characteristic peaks of polyaniline; λ_{max} at 325 nm due to the π-π* transition of the benzenoid rings, a shoulder around 435 nm and a tail extending to the NIR region due to the wellknown polaron transitions[46].

SEM and TEM images of the hybrid P1NH2G2 is shown in figure 6, which shows the presence of polyaniline covered with exfoliated and reduced graphene oxide. HRTEM image showing the lattice fringes of reduced graphene oxide is shown in figure S3.

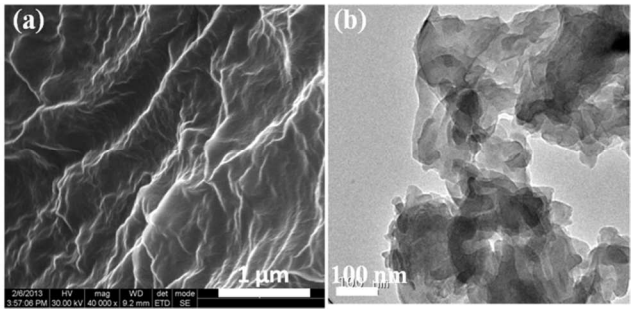

Fig. 6 (a) SEM and (b) TEM images of hybrid P1NH2G2

Room temperature dc-conductivity of polyaniline is observed as 2 S/cm. The hybrid P1NH2G2 shows increased conductivity (6.3 S/cm) than that of pure polyaniline. This may be because of the formation of direct conducting pathways due to the covalent bonds between polyaniline and GONH2. To investigate the effect of phenylenediamine grafting in improving the conductivity, the conductivity of P1NH2G2 is compared with that of polyaniline/GO hybrid (P1G2). P1G2 shows conducitivity less than that of pure polyaniline (0.03 S/cm) because of the insulating nature of GO. After functionalization with phenylenediamine, because of the considerable reduction and exfoliation, GONH2 acts as a conducting filler and the direct covalent linkage between polyaniline and GONH2 promotes easier delocalization of electrons, hence better conductivity. Photoluminescence of the samples in equal weights (1 mg in 5 ml) are recorded in 2-propanol and given in figure 7 (a). Polyaniline shows a broad emission centered at 480 nm. The π-π* transition of the benzenoid units are responsible for the photoluminescence in polyaniline[47]. The excitation wavelength is chosen as 360 nm, since it falls inside the π–π* absorption envelope. After hybridization with polyaniline, the photoluminescence is significantly quenched due to the efficient electron transfer between polyaniline and GONH2 before recombination. Photoluminescence quenching is more significant in P1NH2G2 than in P1G2, revealing better electron transfer through the direct covalent linkage between polyaniline and GONH2 in P1NH2G2. Similiar observation of photoluminescence quenching due to photoinduced electron transfer from P3HT to graphene is reported by Liu Q. et al.[9]

Photoresponse property of the samples under white light illumination is studied by measuring the photocurrent growth and decay of the samples by repetitive switching of the illumination (on/off) at an interval of 30 s. From figure 7 (b) and (c), it is clear that large and efficient photocurrent generation (29 μA) is observed in P1NH2G2, where as polyaniline does not show much higher photocurrent (4.6 μA). The responsivity of the samples are calculated by the equation $(I_{on}-I_{off})/I_{off}$. Pure polyaniline shows a responsivity of 7.8%, while the hybrid shows an increased responsivity of 25.6%. Low exciton dissociation and immediate recombination of the photogenerated electrons and holes is responsible for the low photocurrent in polyaniline. But in the hybrid, the photogenerated exciton may easily be diffused into the interface between polyaniline and reduced graphene oxide and get dissociated. The electrons are transferred to reduced graphene oxide layers and the holes are delocalized along the polyaniline chain and results in large photocurrent. The photocurrent cycles of the hybrids are more reproducible compared to polyaniline. For a comparison, the photocurrent cycles of unfunctionalized GO/polyaniline (P1G2) hybrid is also given in figure 7 (d). It shows only slight improvement in photocurrent (9.1 μA) compared to pure polyaniline. Hence the efficient photocurrent generation of P1NH2G2 is due to the formation of direct conducting pathways because of the covalent linkage between polyaniline reduced graphene oxide sheets.

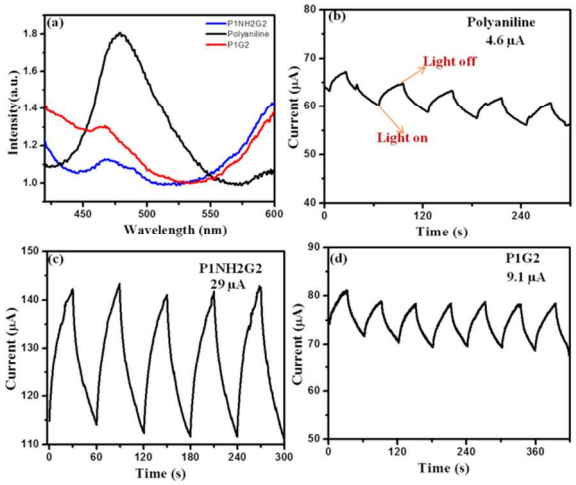

Fig. 7 (a) Photoluminescence spectrum and (b-d) photocurrent cycles of the samples

To get an insight into the process of photocurrent generation in this hybrid, energy level diagram of the photocurrent generating system is drawn as shown in figure 8. The calculated wrokfunction of graphene is approximately 4.4 eV[48]. CV experiments were used to calculate the exact HOMO/LUMO energy levels of polyaniline in the P1NH2G2 hybrid. CV curve is shown in Figure S4 of the Supplimentary Information. HOMO and LUMO energy Levels (E_{HOMO} and E_{LUMO}) of polyaniline were calculated through the following equations using ferrocene as the reference potential (E_{ref}).

$$E_{HOMO} = (-4.8 + E_{ref} - E_{ox})\ eV$$

$$E_{LUMO} = (-4.8 + E_{ref} - E_{red})\ eV$$

On the basis of these equations, the energy levels of HOMO and LUMO for polyaniline in the hybrid were calculated to −5.05 and −4 eV, respectively, yielding a band-gap of 1.05 eV.

Under white light illumination, electrons are excited from the the HOMO to the LUMO level of polyaniline. The exciton then diffuses into the interface between donor and acceptor levels of the hybrid. Due to the difference in LUMO energy levels, there exists a strong electric field at the interface between donor and acceptor, which allows the dissociation of excitons. Reduced graphene oxide is having higher electron affinity, so naturally the dissociated electrons can relax to GONH2 and get transported away from polyaniline. The seperated holes can be delocalized along the polyaniline chain. The electrons and holes are then extracted out at cathode and anode respectively, supported by an internal electrical field generated mainly due to the difference in work function of the electrodes used, as figure 8 (a) and (b) depict.

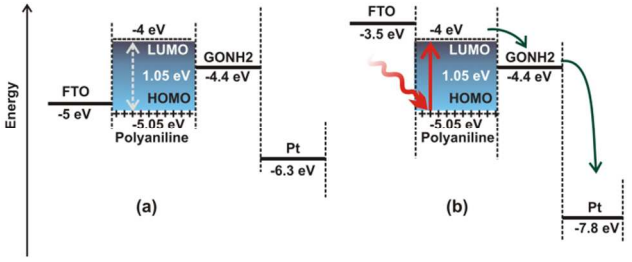

Fig. 8 (a) band alignment of FTO-P1NH2G2-Pt system before the applied bias; (b) band alignment of the system when a bias of 3V is applied across the device and illuminated with light. The arrows show the direction of the photogenerated electrons.

Although the nonlinear optical property of polyaniline-reduced graphene oxide hybrid was reported in our earlier publication[41], the systematic studies on the improved dc-conductivity and photocurrent in polyaniline-GONH2 hybrid in comparison to the pure polyaniline and polyaniline-unfucntionalized GO hybrid is new to the scientific community.

Conclusions

Phenylenediamine functionalized reduced graphene oxide is designed, synthesized and characterized for synthesizing polyaniline hybrids with direct covalent connectivity to reduced graphene oxide sheets. The hybrid shows around 3 times increase in electrical conductivity compared to pure polyaniline and around 200 times increase with respect to unfunctionalized GO/polyaniline hybrid. Considerable reduction and exfoliation of GO after phenylenediamine grafting and the covalent bonds between polyaniline and GONH2 are responsible for the better conductivity. Significant photoluminescence quenching is observed in the hybrid and is due to the efficient electron transfer between polyaniline and GONH2. The hybrid produces large and stable photocurrent under white light irradiation and hence it is an interesting material for optoelectronic applications.

Aknowledgements

One of the author RT thank IIST for providing IIST-ISRO research fellowship and Dr. Jinesh K. B., Assistant Professor, Department of Physics, IIST for the discussions related to photocurrrent measurements. Authors thank SAIF, IITM for SEM studies and NIIST, Trivandrum for TEM measurements.

Notes and references

[a] *Department of Chemistry, Indian Institute of Space Science and Technology, Valiamala, Thiruvananthapuram, Kerala, India. Fax: +91471 2568541; Tel: +91471 2568536; E-mail:honey@iist.ac.in*
[b] *Department of Physics, Indian Institute of Space Science and Technology, Valiamala, Thiruvananthapuram, Kerala, India. Fax: +91471 2568542; Tel: +91471 2568552; E-mail:pramod@iist.ac.in*

† Electronic Supplementary Information (ESI) available: [Fig. S1. FTIR spectrum of polyaniline. Fig. S2. XRD spectrum of polyaniline. Fig. S3. HRTEM image of the hybrid. Fig. S4 CV of P1NH2G2 in 0.1 M NaCl at a scan rate of 100 mV/s]. See DOI: 10.1039/b000000x/

1. A. K. Geim, K. S. Novoselov, Nat. Mater., 2007, 6, 183 - 191.
2. K. S. Novoselov, A. K. Geim, S. V. Morozov, D. Jiang, Y. Zhang, S. V. Dubonos, I. V. Grigorieva and A. A. Firsov, Science, 2004, 306, 666-669.
3. Z. Liu, Q. Liu, Y. Huang, Y. Ma, S. Yin, X. Zhang, W. Sun and Y. Chen, Adv. Mater., 2008, 20, 3924-3930.
4. J. C. Charlier, X. Gonze and J. P. Michenaud, Phys. Rev.B, 1991, 43, 4579-4589.
5. F. Schedin, A. K. Geim, S. V. Morozov, E. W. Hill, P. Blake, M. I. Katsnelson and K. S. Novoselov, Nat. Mater., 2007, 6, 652-655.
6. J. R. Williams, L. DiCarlo and C. M. Marcus, Science, 2007, 317, 638-641.
7. Y. Li, S. Li, L. Jin, J.B. Murowchick and Z. Peng, RSC Adv., 2013, 3, 16308-16312.
8. X. Zhang, F. Wang, H. Huang, H. Li, X. Han, Y. Liu and Z. Kang, Nanoscale, 2013, 5, 2274-2278.
9. Q. Liu, Z. Liu, X. Zhang, L. Yang, N. Zhang, G. Pan, S. Yin, Y. Chen and J. Wei, Advanced Functional Materials, 2009, 19, 894-904.
10. X. Li, W. Cai, J. An, S. Kim, J. Nah, D. Yang, R. Piner, A. Velamakanni, I. Jung, E. Tutuc, S. K. Banerjee, L. Colombo and R. S. Ruoff, Science, 2009, 324, 1312-1314.
11. D. Li, M. B. Muller, S. Gilje, R. B. Kaner and G. G. Wallace, Nat. Nano, 2008, 3, 101-105.
12. C. Zhu, S. Guo, Y. Fang and S. Dong, ACS Nano, 2010, 4, 2429-2437.
13. M. Zhou, Y. Wang, Y. Zhai, J. Zhai, W. Ren, F. Wang and S. Dong, Chem. Eur. J., 2009, 15, 6116-6120.
14. H.-L. Guo, X.-F. Wang, Q.-Y. Qian, F.-B. Wang and X.-H. Xia, ACS Nano, 2009, 3, 2653-2659.
15. W. S. Hummers and R. E. Offeman, J. Am. Chem. Soc., 1958, 80, 1339-1339.
16. S. Stankovich, R. D. Piner, S. T. Nguyen and R. S. Ruoff, Carbon, 2006, 44, 3342-3347.
17. Y. Si and E. T. Samulski, Nano Lett., 2008, 8, 1679-1682.
18. S. Niyogi, E. Bekyarova, M. E. Itkis, J. L. McWilliams, M. A. Hamon and R. C. Haddon, J. Am. Chem. Soc., 2006, 128, 7720-7721.
19. S. Guo, S. Dong and E. Wang, ACS Nano, 2009, 4, 547-555.
20. B.-S. Kong, J. Geng and H.-T. Jung, Chem. Commun., 2009, 2174-2176.
21. X. Huang, X. Zhou, S. Wu, Y. Wei, X. Qi, J. Zhang, F. Boey and H. Zhang, Small, 2010, 6, 513-516.
22. S. Chen, J. Zhu, X. Wu, Q. Han and X. Wang, ACS Nano, 2010, 4, 2822-2830.
23. M. K. Kavitha, H. John, P. Gopinath and R. Philip, J. Mater. Chem. C, 2013, 1, 3669-3676.
24. P. Nayak, B. Anbarasan and S. Ramaprabhu, J. Phys. Chem. C, 2013, 117, 13202-13209.
25. A. Cao, Z. Liu, S. Chu, M. Wu, Z. Ye, Z. Cai, Y. Chang, S. Wang, Q. Gong and Y. Liu, Adv. Mater., 2010, 22, 103-106.
26. C.-Y. Liu, K.-C. Huang, P.-H. Chung, C.-C. Wang, C.-Y. Chen, R. Vittal, C.-G. Wu, W.-Y. Chiu and K.-C. Ho, J. Power Sources, 2012, 217, 152-157.
27. L. Jianhua, A. Junwei, Z. Yecheng, M. Yuxiao, L. Mengliu, Y. Mei and L. Songmei, ACS Appl. Mater. Interfaces, 2012, 4, 2870-2876.
28. F. Alvi, M. K. Ram, P. A. Basnayaka, E. Stefanakos, Y. Goswami and A. Kumar, Electrochim. Acta, 2011, 56, 9406-9412.

29. S.-S. Li, K.-H. Tu, C.-C. Lin, C.-W. Chen and M. Chhowalla, ACS Nano, 2010, 4, 3169-3174.
30. Q. Liu, Z. Liu, X. Zhang, L. Yang, N. Zhang, G. Pan, S. Yin, Y. Chen and J. Wei, Adv. Fun. Mater. 2009, 19, 894-904.
31. P. Schilinsky, C. Waldauf and C. J. Brabec, Appl. Phys. Lett., 2002, 81, 3885-3887.
32. Z. Liu, D. He, Y. Wang, H. Wu and J. Wang, Solar Energ. Mater. Sol. C., 2010, 94, 1196-1200.
33. N. Karousis, A. S. D. Sandanayaka, T. Hasobe, S. P. Economopoulos, E. Sarantopoulou and N. Tagmatarchis, Journal of Materials Chemistry, 2011, 21, 109-117.
34. J. Tang, L. Niu, J. Liu, Y. Wang, Z. Huang, S. Xie, L. Huang, Q. Xu, Y. Wang and L. A. Belfiore, Materials Science and Engineering: C, 2014, 34, 186-192.
35. J. An, J. Liu, Y. Zhou, H. Zhao, Y. Ma, M. Li, M. Yu and S. Li, The Journal of Physical Chemistry C, 2012, 116, 19699-19708.
36. L. Jianhua, A. Junwei, Z. Yecheng, M. Yuxiao, L. Mengliu, Y. Mei and L. Songmei, ACS Applied Materials & Interfaces, 2012, 4, 2870-2876.
37. M. Kumar, K. Singh, S. K. Dhawan, K. Tharanikkarasu, J. S. Chung, B.-S. Kong, E. J. Kim and S. H. Hur, Chemical Engineering Journal, 2013, 231, 397-405.
35. 38. N. A. Kumar, H.-J. Choi, Y. R. Shin, D. W. Chang, L. Dai and J.-B. Baek, ACS Nano, 2012, 6, 1715-1723.
39. Z.-F. Li, H. Zhang, Q. Liu, Y. Liu, L. Stanciu and J. Xie, Carbon, 2014, 71, 257-267.
40. B. Zhang, Y. Chen, Y. Ren, L.-Q. Xu, G. Liu, E.-T. Kang, C. Wang, C.-X. Zhu and K.-G. Neoh, Chemistry – A European Journal, 2013, 19, 6265-6273.
41. T. Remyamol, H. John and P. Gopinath, Carbon, 2013, 59, 308-314.
42. W. Sun, S. Shi and T. Yao, Analytical Methods, 2011, 3, 2472-2474.
43. G. Wang, Z. Yang, X. Li and C. Li, Carbon, 2005, 43, 2564-2570.
44. L. M. Malard, M. A. Pimenta, G. Dresselhaus and M. S. Dresselhaus, Phys. Rep., 2009, 473, 51-87.
45. H. C. Schniepp, J. Phys. Chem. B, 2006, 110, 8535-8539.
46. J. Stejskal, P. Kratochvíl and N. Radhakrishnan, Synthetic Metals, 1993, 61, 225-231.
47. J. Y. Shimano and A. G. MacDiarmid, Synthetic Metals, 2001, 123, 251-262.
48. R. Czerw, B. Foley, D. Tekleab, A. Rubio, P. M. Ajayan and D. L. Carroll, Phys. Rev. B, 2002, 66, 033408.